Crystal Structures of the *Bacillus licheniformis* BS3 Class A β-Lactamase and of the Acyl−Enzyme Adduct Formed with Cefoxitin[†,‡]

Eveline Fonzé,*,[§] Marc Vanhove,[‖] Georges Dive,[‖] Eric Sauvage,[§] Jean-Marie Frère,[‖] and Paulette Charlier[§]

*Centre d'Ingénierie des Protéines, Institut de Physique B5 and Institut de Chimie B6, Université de Liège,
B-4000 Sart Tilman, Belgium*

ABSTRACT: The *Bacillus licheniformis* BS3 β-lactamase catalyzes the hydrolysis of the β-lactam ring of penicillins, cephalosporins, and related compounds. The production of β-lactamases is the most common and thoroughly studied cause of antibiotic resistance. Although they escape the hydrolytic activity of the prototypical *Staphylococcus aureus* β-lactamase, many cephems are good substrates for a large number of β-lactamases. However, the introduction of a 7α-methoxy substituent, as in cefoxitin, extends their antibacterial spectrum to many cephalosporin-resistant Gram-negative bacteria. The 7α-methoxy group selectively reduces the hydrolytic action of many β-lactamases without having a significant effect on the affinity for the target enzymes, the membrane penicillin-binding proteins. We report here the crystallographic structures of the BS3 enzyme and its acyl−enzyme adduct with cefoxitin at 1.7 Å resolution. The comparison of the two structures reveals a covalent acyl−enzyme adduct with perturbed active site geometry, involving a different conformation of the Ω-loop that bears the essential catalytic Glu166 residue. This deformation is induced by the cefoxitin side chain whose position is constrained by the presence of the α-methoxy group. The hydrolytic water molecule is also removed from the active site by the 7β-carbonyl of the acyl intermediate. In light of the interactions and steric hindrances in the active site of the structure of the BS3−cefoxitin acyl−enzyme adduct, the crucial role of the conserved Asn132 residue is confirmed and a better understanding of the kinetic results emerges.

β-Lactam antibiotics are widely used in antimicrobial therapy because of their ability to inactivate DD-transpeptidases and/or DD-carboxypeptidases, also called penicillin-binding proteins (or PBPs),[1] which are essential enzymes in bacterial cell wall synthesis. The natural substrates of these enzymes are structurally similar to β-lactam-based compounds.

An important phenomenon of resistance is caused by the bacterial production of β-lactamases that rapidly hydrolyze β-lactams and release inactive products. On the basis of their catalytic mechanisms, β-lactamases are divided into two groups. The first includes zinc enzymes that are indexed as class B enzymes. All the other β-lactamases fall into a second group of "active site" serine enzymes and together with PBPs form the "penicilloyl serine transferase" superfamily (*1*). According to their amino acid sequences, the serine β-lactamases are subdivided into three classes (A, C, and D), but they all follow a similar kinetic pathway schematically represented by a simple three-step model:

$$E + S \underset{k_{-1}}{\overset{k_1}{\rightleftharpoons}} ES \xrightarrow{k_2} ES^* \xrightarrow{k_3} E + P$$
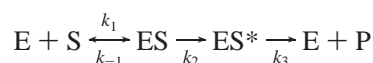
where E is the enzyme, S the substrate, ES a noncovalent Henri−Michaelis complex, ES* a covalent acyl−enzyme adduct, and P the inactive degradation product of the substrate. Usually, this reaction is characterized by the classical Henri−Michaelis parameters k_{cat} and K_m describing the maximum rate of hydrolysis and the substrate affinity, respectively. Therefore, an efficient β-lactamase exhibits high k_{cat} and k_{cat}/K_m values, the latter reflecting the rate of acylation. The same kinetic scheme applies to the interaction between PBPs and β-lactams, but the value of k_3 is very low. The ideal therapeutic antibiotic would thus combine very low k_{cat} values with both PBPs and β-lactamases or, even better, would not be recognized by the latter enzymes (very low k_{cat}/K_m), while exhibiting a sufficient k_2/K' value (where $K' = k_1 + k_2/k_1$), at least 10^3 M^{-1} s^{-1} with PBPs.

Compared to "classical" cephems, cefoxitin, a semisynthetic antibiotic, exhibits considerably decreased rates of both acylation and deacylation with many class A β-lactamases, whereas its affinity for most PBPs remains almost unchanged (*2*). With class C β-lactamases, the acylation is rather efficient, but the deacylation rate is slow (*3*). This behavior is generally observed with compounds bearing a methoxy side chain on the α-face of the β-lactam ring (Table 1). Representative of the cephamycin group of antibiotics, cefoxitin extends its antibacterial spectrum to many cephalosporin-resistant Gram-negative bacteria. Several kinetic and modeling studies have already been performed on the

---

* To whom correspondence should be addressed. Phone: 32 43 66 36 19. Fax: 32 43 66 47 41. E-mail: eveline.fonze@ulg.ac.be.

[§] Institut de Physique B5.

[‖] Institut de Chimie B6.

[1] Abbreviations: PBPs, penicillin-binding proteins; NMR, nuclear magnetic resonance; PDB, Protein Data Bank; rms, root-mean-square.

Table 1: Structure of Substrates and Kinetic Parameters Discussed in This Study

Substrates	R	R'	R"	k_{cat}/K_m[a]
Cefoxitin	(thiophene)CH_2-	$-O-CO-NH_2$	$-OCH_3$	1
Cephalothin	(thiophene)CH_2-	$-O-CO-CH_3$	$-H$	24.10^4
Moxalactam[b]	(HO-phenyl)$CH-$, COO^-	$-S-$(tetrazole-$N-CH_3$)	$-OCH_3$	6
FMCA[c]	$H-$	$-O-C-CH_3$	$-OCH_3$	10

[a] Kinetic parameters were determined at 30 °C on the BS3 β-lactamase in 100 mM sodium citrate (pH 5.0). [b] The structure of moxalactam contains an oxygen atom instead of a sulfur atom in position 1. [c] FMCA is 7β-formamidoyl-7α-methoxycephalosporanic acid. Kinetic parameters for this compound were determined on the *B. licheniformis* 749/C β-lactamase at pH 7.0 (4).

reactions between various β-lactamases and compounds bearing α-methoxy and C-3' groups (2–7). They first showed that the interaction between the *Escherichia coli* TEM-1 class A β-lactamase and cefoxitin induced deformation of the active site (5). This result was later confirmed by NMR experiments on the acyl−enzyme adduct formed by the β-lactamases of *Bacillus licheniformis* 749/C and cefoxitin (4). It was also demonstrated that the kinetic pathway of a class A β-lactamase with cefoxitin could be somehow modified compared to the three-step model described above. Formation of a second, more stable, acyl−enzyme ES** results from the elimination of the C-3' leaving group from ES*. When this reaction is as fast as or faster than the formation of ES*, the modified ES** adduct is the most abundant steady-state intermediate (4, 6, 7). Molecular modeling studies of cefoxitin with the β-lactamases from *Streptomyces albus* G and *B. licheniformis* 749/C indicated that the α-methoxy group of the substrate induced a displacement of the so-called hydrolytic water molecule, explaining the very low hydrolysis rates (7).

Here we report the 1.7 Å resolution crystal structures of the BS3 β-lactamase and of its adduct with cefoxitin. The complex is an acyl−enzyme intermediate where the C-3' leaving group of cefoxitin has been eliminated. A comparison with the unliganded BS3 structure clearly reveals significant conformational modifications, arising from the adaptation of the catalytic pocket Ω-loop to the steric hindrance of the substrate 7β side chain. Our results confirm also the crucial role of the conserved Asn132 residue for an adequate positioning of β-lactam substrates.

MATERIALS AND METHODS

Protein Purification, Crystallization, and Data Collection. The expression and purification of the BS3 enzyme were performed according to the method of Ledent and co-workers (8). The initial crystallization conditions for the BS3 enzyme were determined using the Gridscreen, Crystalscreen, and Crystalscreen II sparse matrix crystallization kits (Hampton Research). Orthorhombic crystals were first obtained using the hanging drop vapor diffusion method with drops containing 5 μL of a protein solution (10 mg/mL) and 5 μL of 25%

PEG 6000 in 100 mM sodium acetate buffer (pH 5.0), equilibrated against 1 mL of the latter solution at 20 °C. Monoclinic crystals were then obtained when the buffer solution was changed to 100 mM sodium citrate (pH 5.0). By increasing the protein concentration to 40 mg/mL and lowering the PEG 6000 concentration and the pH of the buffer to 10% and 3.4, respectively, we obtained very big prismatic crystals of up to 1.0 mm^3. The BS3−cefoxitin adduct was obtained by diffusing into the crystals increasing concentrations of cefoxitin over the course of 24 h at room temperature. A fresh solution of cefoxitin was continuously added up to a final concentration of 25 mM.

The first X-ray diffraction spectrum was obtained from orthorhombic crystals collected at room temperature using a Siemens X1000 area detector system with a conventional rotating-anode generator as the X-ray source. This single crystal, belonging to space group $P2_12_12_1$ with unit cell dimensions $a = 54.97$ Å, $b = 87.03$ Å, and $c = 110$ Å, and containing two molecules per asymmetric unit, diffracts to only 2.4 Å resolution (8). All data with monoclinic crystals, BS3 and the BS3−cefoxitin adduct, were collected at room temperature at LURE (Orsay, France) on beamline D41A at a wavelength of 1.375 Å using a Mar-Research image plate detector. Indexing and integration were carried out using MOSFLM version 5.41 (9), and the scaling of the intensity data was accomplished with SCALA of the CCP4 program suite (10). These crystals diffracted to 1.65 Å resolution, and data statistics are given in Table 2. As the orthorhombic form, the monoclinic crystals contain two molecules per asymmetric unit but are characterized by a higher solvent content, roughly 51% versus 40% for the orthorhombic form according to Matthews's coefficient (11).

Structure Determination and Refinement. As the amino acid sequences of BS3 and of the *B. licheniformis* 749/C β-lactamase (12) (PDB entry 4BLM) differ by only seven residues, the structure of BS3 was determined by molecular replacement with the AMORE package (13) using data of the monoclinic crystals. The starting model was composed of only one monomer of the 749/C structure, with water molecules removed. The model was refined by simulated annealing in X-PLOR (14) with a $\sigma(F)$ cutoff of 2.0. At each

Table 2: X-ray Data Collection[a]

	BS3	BS3−cefoxitin
space group	$P2_1$	$P2_1$
cell parameters:		
β (deg)	94.43	94.18
a, b, c (Å)	47.36, 106.82, 63.90	47.34, 106.37, 63.87
resolution (Å)	23.74−1.65 (1.97−1.65)	22.03−1.65 (1.97−1.65)
no. of measurements	165623 (64168)	143995 (54861)
no. of unique reflections	70471 (27770)	68766 (26718)
completeness (%)	93.3 (89.7)	91.8 (87.1)
average $I/\sigma(I)$	5.4 (4.9)	5.0 (2.1)
R_{merge}[b] (%)	4.8 (17.0)	7.2 (43.0)

[a] Data for the highest-resolution shell are in parentheses. [b] $R_{merge}(I) = \sum_{hlk}|I_{hlk} - \langle I_{hkl}\rangle|/\sum_{hlk}I_{hkl}$, where I_{hkl} is the measured intensity of the reflection with indices hkl.

step of refinement (positions and temperature factors), the $2F_o - F_c$ and $F_o - F_c$ electron density maps were calculated using X-PLOR, and manual rebuilding was done in the program TURBO-FRODO (15).

To determine the structure of the BS3−cefoxitin complex, the dimer of the unliganded BS3 enzyme without active site solvent molecules was used as the initial phasing model. After rigid body refinement, the resulting model was used to calculate the $2F_o - F_c$ and $F_o - F_c$ maps, which revealed perturbations of the Ω-loop defining a side of the catalytic pocket, and a covalent bond between the active serine and the substrate. The Ω-loop was rebuilt using an omit map which excluded residues 166−170, and the cefoxitin was built into the observed difference density. The complexed structure was refined as the unliganded one, by several alternating cycles of simulated annealing in X-PLOR and model refitting in TURBO-FRODO.

For both structures, the two molecules of the asymmetric unit were treated independently, without averaging, to identify different eventual conformations. All atoms were refined with an occupancy of 1.0, and only the first layer of water molecules having a very well-defined electron density and a temperature factor of <50.0 Å² was considered. The free enzyme and adduct structures were refined to 1.7 Å with R_{free} values of 23.5 and 25.6%, respectively. The statistics of refinement are summarized in Table 3. Atomic coordinates have been deposited in the Protein Data Bank (entries 1I2S and 1I2W).

Citrate and Cefoxitin Parametrization. To include small compounds (such as citrate in the free enzyme and cefoxitin in the adduct) during the refinement processes, the topology and parameter files suitable for X-PLOR had to be generated. To do so, the small compounds were first constructed and fitted in the electron density maps. All the degrees of freedom describing the molecular geometry were then fully optimized at the ab initio quantum chemistry level with the minimal basis set MINI-1′ of Huzinaga (16, 17) using the minimization procedures available in the Gaussian suite of programs (18). The net charges were derived from Mulliken's population analysis scheme.

Determination of Kinetic Parameters. Benzylpenicillin was from Rhône-Poulenc, and cephalothin, cefoxitin, and moxalactam were from Sigma. Kinetic parameters were determined at 30 °C in the indicated buffers. Complete time

Table 3: Refinement Statistics

	BS3	BS3−cefoxitin
resolution range (Å)	8.0−1.7	8.0−1.7
completeness (working + test) (%)	94.1	92.6
no. of reflections ($F > 2\sigma$)	64762	63397
R[a] (working set)/R_{free} (test set) (%)	19.7/23.5	21.6/25.6
R_{free} (test set size) (%)	5.1	5.1
estimated error in the R_{free} value	0.004	0.005
no. of protein atoms (non-hydrogen)	3990	3999
no. of ligand and solvent atoms (non-hydrogen)	180	181
B values from the Wilson plot (Å²)	21.4	23.1
mean B value (Å²)		
overall	24.0	25.1
protein atoms	23.6	24.9
solvent atoms	32.6	32.0
cefoxitin atoms	−	24.2
estimated coordinate error		
(low-resolution cutoff of 5.0 Å)		
Luzzati plot/σA (Å)	0.20/0.19	0.23/0.28
rms deviations from ideal values		
bond lengths/bond angles (Å/deg)	0.006/1.3	0.007/1.3
dihedral angles/improper angles (deg/deg)	25.3/0.69	25.4/0.96

[a] $R = \sum_{hlk}||F_{ohkl}| - |F_{chkl}||/\sum_{hlk}F_{ohkl}$, where $|F_{ohkl}|$ and $|F_{chkl}|$ are the observed and calculated structure factor amplitudes, respectively, for reflection hkl belonging to the working set. R_{free} is defined for reflection hkl belonging to the test set.

courses of the hydrolysis of cephalothin and benzylpenicillin were recorded at 260 and 235 nm, respectively, and the k_{cat}/K_m values for these compounds were derived as described by De Meester and co-workers (19). Hydrolysis of cefoxitin and moxalactam was followed at 273 and 270 nm, respectively, and k_{cat}/K_m values were obtained from initial rates of hydrolysis at substrate concentrations well below the K_m (typically 100 μM).

RESULTS

Overall Structure of the BS3 Enzyme. The crystallographic structure of BS3 was determined to 1.7 Å resolution (Table 3) by molecular replacement using as a search model the structure of the homologous β-lactamase of *B. licheniformis* 749/C (12). The BS3 crystal reveals two molecules per asymmetric unit, which were refined independently with 260 amino acid residues. When compared, the two monomers are very similar with an rms deviation of 0.22 Å between the equivalent backbone atoms (N, Cα, C, and O atoms). As expected, the BS3 polypeptide chain exhibits the typical fold of all known class A β-lactamases and is composed of two globular domains. One domain is formed by a long central α-helix (α2) surrounded by four α-helices (α4−α6 and α9) and four 3_{10}-helices (α30−α32 and α7). Just before the helix α2, a one-turn 3_{10}-helix (α20) is formed. The second domain consists of a five-stranded antiparallel β-sheet (β1−β5) covered by the N- and C-terminal α-helices (α1 and α11) and a short α-helix (α10) on one face and one α-helix (α8) on the other face (Figure 1a).

The catalytic pocket is located at the interface between the two domains. It is limited by four structural elements well conserved among all class A β-lactamase structures. The center of the substrate cavity is occupied by the Ser70-Thr71-Ile72-Lys73 tetrad, including the nucleophilic serine residue. One side of the cavity is defined by the Ser130-Asp131-Asn132 loop, and the opposite side consists of the
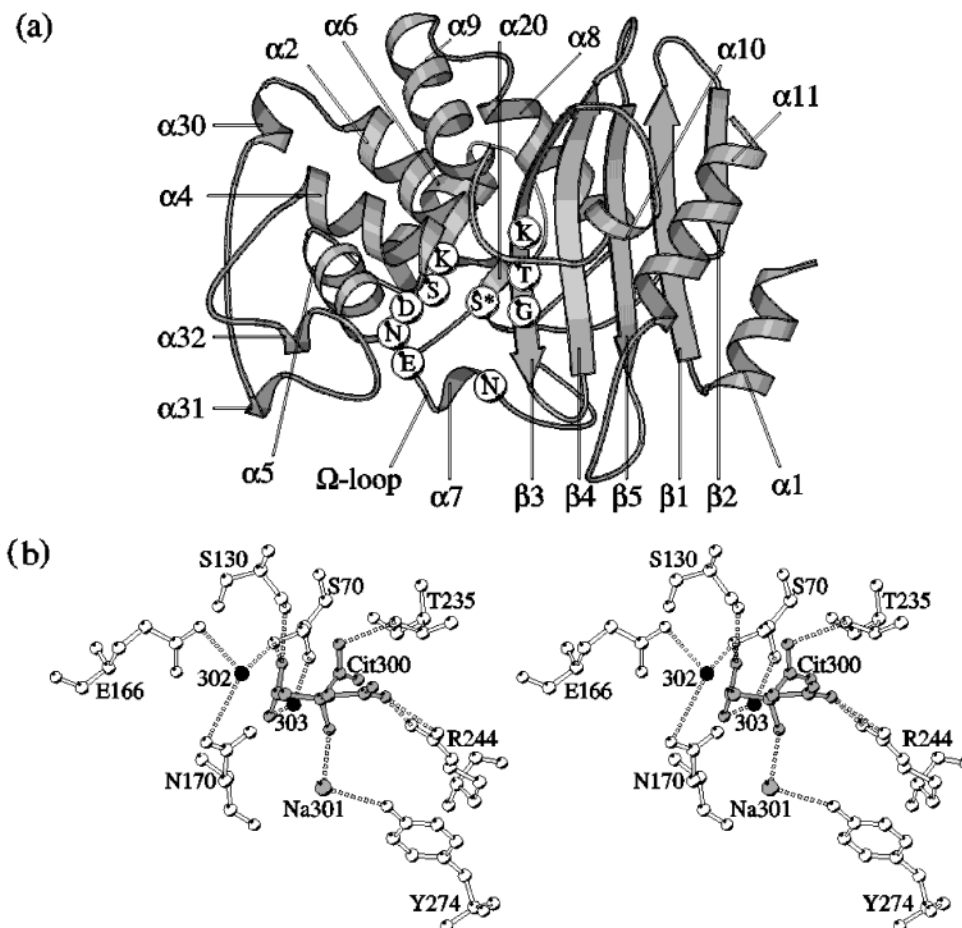
FIGURE 1: (a) Ribbon diagram of the BS3 β-lactamase with secondary structure assignments computed with the program DSSP (*20*) and identification of the conserved residues of the active site, including the nucleophilic serine S* residue. (b) Stereoview of the active site of BS3 with the two essential water molecules, Wat302 and Wat303 (black). The other solvent molecules are denoted Cit300 and Na301 for the citrate and Na$^+$ ions (gray), respectively, and their hydrogen bonds are represented by dashed lines. This figure was produced using MolScript (*21*).

Lys234-Thr235-Gly236 triad on strand β3. The bottom is closed by an Ω-loop bearing helix α7, and containing the Glu166 and Asn170 residues that point into the active site.

Maps constructed with data from 20 to 1.7 Å clearly showed a significant electron density in the catalytic cleft of each monomer that can be attributed to one citrate anion resulting from crystallization conditions (Figure 2a). As observed in other β-lactamase crystallographic structures, where sulfate or acetate ion is also present in the catalytic pocket, citrate has no impact on the active site structure. The citrate molecule interacts with the hydroxyl oxygen atoms of both Ser70 and Ser130 residues and with a Na$^+$ ion or a water molecule, which is itself in contact with the Tyr274 hydroxyl group. Citrate also interacts with the side chains of Thr235 and Arg244, both bordering the active site and generally considered to be involved in the positioning of substrates (Figure 1b). Those multiple interactions can explain the different kinetic results observed when experiments are performed in sodium acetate or citrate. With cephalothin at pH 5 in either 100 mM sodium acetate or 100 mM sodium citrate, kinetic experiments reveal K_m values of 42 μM or higher than 1 mM, respectively, with unchanged V_{max} values, suggesting that citrate ions behave as competitive inhibitors.

The BS3 crystal structure is also solvated by 152 ordered water molecules. Two of these solvent molecules, mainly

located in the first coordination shell, are very well conserved in all class A β-lactamase structures. Wat302, the so-called hydrolytic class A water molecule, interacts with the active Ser70 and Glu166 of the Ω-loop. The other conserved molecule, Wat303, interacts with the oxyanion hole formed by the NH groups of the Ala237 and nucleophilic Ser70 residues, and also with an oxygen atom of a carboxylate group of the citrate ion.

Comparison with the B. licheniformis 749/C β-Lactamase. Since the amino acid sequences of *B. licheniformis* 749/C and BS3 differ by only seven point mutations, the structures of the two enzymes are very similar with an rms deviation of $\sim$0.36 Å^2 between the equivalent backbone atoms. According to the ABL numbering (*22*), six mutations (Ala59 → Thr, Val187 → Ala, Arg191 → Gln, Asp227 → Glu, Ala238 → Gly, and Met287 → Leu) occur in the α/β-domain, and one occurs in the α-domain at the N-terminal α5 helix (Ala133 → Thr) (*23*). Residues 59, 191, and 227 are on the surface of the protein and do not exhibit any significant interaction either in BS3 or in 749/C. Residues 133, 187, and 287 are completely buried, and the latter two are involved in hydrophobic clusters. The replacement of Met287 in 749/C with the smaller Leu in the BS3 leads to a slight displacement of the polypeptide chain of the α10–β3 loop and of residues 250–253, just after strand β4. Similarly, the Thr133 → Ala mutation also induces a small shift of residues 100–104.
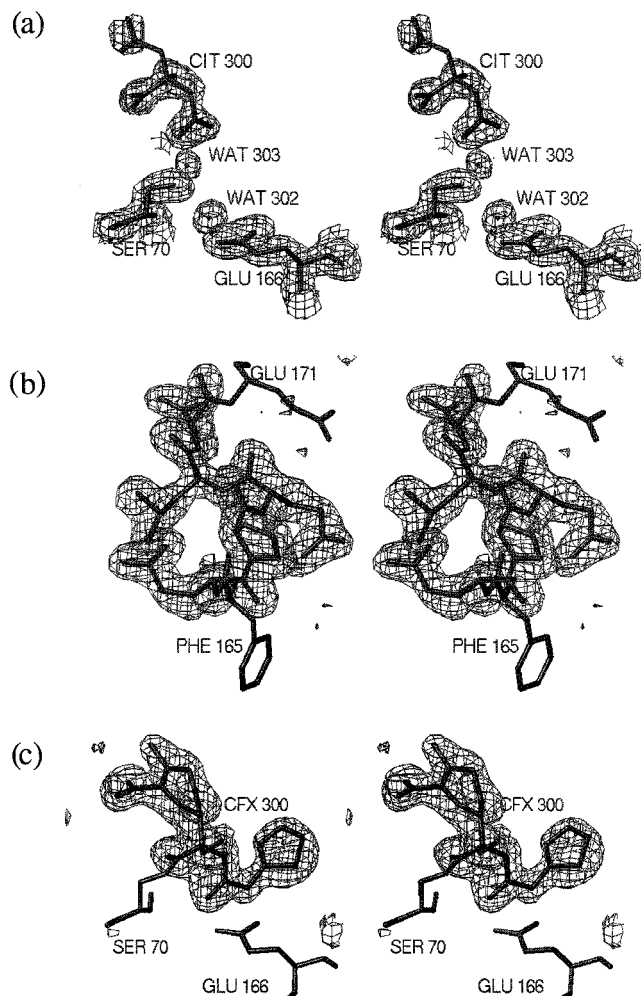
FIGURE 2: (a) Stereoview of the $2F_o - F_c$ electron density map (contoured at the 1.4σ level) of the unliganded BS3 enzyme showing the two essential water molecules (WAT 302 and WAT 303) and the citrate ion (CIT 300) in the active site. (b) Stereoview of the $F_o - F_c$ electron density map of the BS3−cefoxitin adduct showing the Ω-loop region of residues 165−171. Atoms from residues 166 to 170 of each monomer were omitted from the F_c calculation, and the contour level is 3.0σ. (c) Stereoview of the $F_o - F_c$ electron density map of the BS3−cefoxitin adduct with the cefoxitin moiety (CFX 300) covalently bound to the active serine (SER 70). The cefoxitin atoms of each monomer were omitted from the F_c calculation, and the contour level is 3.0σ.

Residue 187 participates in a spatially aligned triad in BS3 (Thr59, Phe47, and Ala187) and in 749/C (Ala59, Phe47, and Val187), with two sterically compensating mutations. The last mutation (Ala238 → Gly) is on strand $\beta3$, limiting the active site. The side chain of the alanine 238 residue points to the bottom of the catalytic pocket. Its small size and lack of polar or charged properties do not allow major interactions with substrates. The substitution of an alanine in position 238 with a glycine residue does not perturb the active site geometry and is unlikely to modify significantly the enzymatic activity profile.

BS3−Cefoxitin Structure. The crystal structure of the BS3−cefoxitin adduct was also determined by molecular replacement, and the two molecules occupying the asymmetric unit were refined separately to 1.7 Å resolution (Table 3). As for the free enzyme, the two monomers are very similar (with an rms deviation of 0.26 Å between the equivalent backbone atoms) and their active sites nearly

superimposable; the following discussion only refers to the structure of one monomer. The overall structure of the adduct closely resembles that of the free enzyme (with an rms deviation of 0.26 Å between the equivalent N, Cα, C, and O atoms) except for the N- and C-terminal residues [Gly238−Ser240, Pro254 and Lys255, and especially Pro167−Val172 (Figure 2b)]. The rms deviation of these backbone regions is 2 or 3 times larger than the overall rms deviation which is within the range of experimental error. The N-terminal Asp31 and Asp32 residues, the C-terminal Ala289, and the Pro254 and Lys255 residues of the $\beta4-\beta5$ loop are all far from the active site and their side chains totally exposed to the solvent without any constraint due to atoms of their own or symmetric molecules. Their positions are also different in the *B. licheniformis* 749/C β-lactamase. By contrast, the Pro167−Val172 region includes a portion of the Ω-loop that borders the catalytic cleft, and the different conformation observed in the adduct structure is a direct consequence of cefoxitin binding (Figure 3). This new Ω-loop conformation also induces a slight displacement of the lower part of strand $\beta3$ defined by the Gly238 and Ser240 residues.

The electron density in the adduct crystal structure unambiguously reveals a covalent acyl−enzyme adduct where cefoxitin has lost its C-3′ leaving group (Figure 2c). Carbonyl O9 of the open β-lactam ring replaces Wat303 in the oxyanion hole at a distance of 2.9 Å from both main chain nitrogens of Ser70 and Ala237 (Figure 4a). The cefoxitin carboxylate oxygen atoms form only one hydrogen bond to Thr235 OG1 at a distance of 2.6 Å (Table 4).

In all known high-resolution acyl−enzyme structures of the penicilloyl serine transferase family, a similar binding mode of the 7(or 6)β-amido linkage of cephalosporins (or penicillins) is observed. In the acyl−enzyme adduct formed by penicillin G and the TEM-1 Glu166 → Asn inactive mutant (*24*) (PDB entry 1FQG), the 6β-amido nitrogen and oxygen atoms are hydrogen bonded to the main chain carbonyl oxygen atom of Ala237 and to the amide nitrogen atom of Asn132, respectively (Figure 4b). With phosphonate or boronate inhibitors displaying an amidated side chain, the same type of orientation is also found, in class A (*25−27*) (PDB entries 1BLH, 1AXB, 1ERM, 1ERQ, and 1ERO) or class C (*28−30*) (PDB entries 1BLS, 1FSY, and 1IEM) β-lactamases. The acyl−enzyme adducts formed by either the class C β-lactamase from *E. coli* AmpC and ceftazidime or loracarbef (*30, 31*) (PDB entries 1IEL and 1FCN) or the DD-carboxypeptidase from *Streptomyces* R61 and cephalosporin C (*32*), cephalothin, or cefotaxime (*33*) (PDB entries 1CEG and 1CEF) also exhibit similar binding schemes between the 7β-amido group and Ala318 or Thr301 (equivalent to class A residue 237) and Asn152 or Asn161 (equivalent to class A residue 132). In the BS3−cefoxitin acyl−enzyme adduct, the steric constraints between the Asn132 side chain and the methoxy group on the α-face of the β-lactam ring force this group further into the catalytic pocket, where it interacts with the Ser70 and Lys73 residues. Because of the tetrahedral character of C7 and the steric bulk of the methoxy group, the 7β side chain can no longer adopt the typical conformation characterized by the interactions involving the peptide-like moiety (N and O) of the cefoxitin side chain and the Asn132−Ala237 pair. The 7β-carbonyl points into the active site in such a way that the oxygen atom
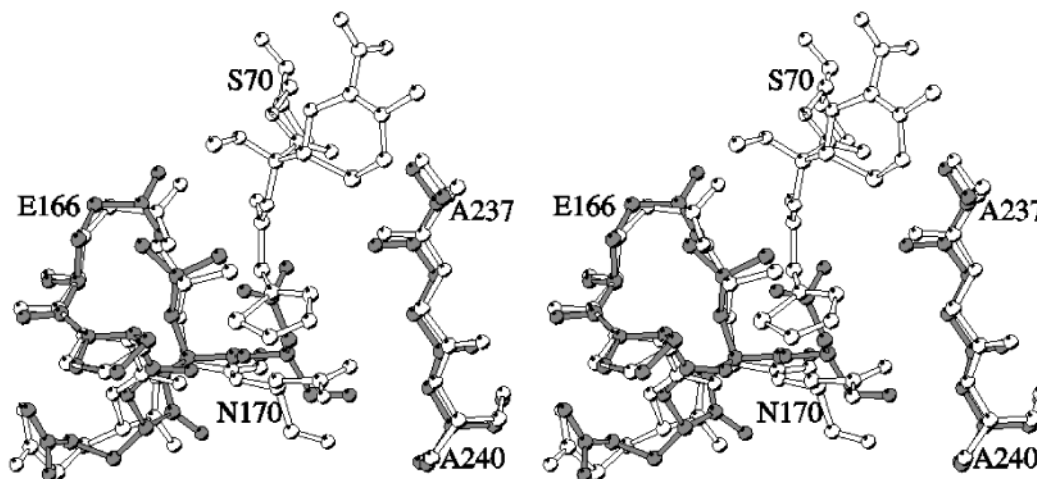
FIGURE 3: Superimposed active sites of the unliganded BS3 enzyme (gray) and of the acyl−enzyme adduct with cefoxitin (white), showing the Ω-loop (E166−N170) deformation and the shift of strand β3 (A237−A240) induced by cefoxitin.
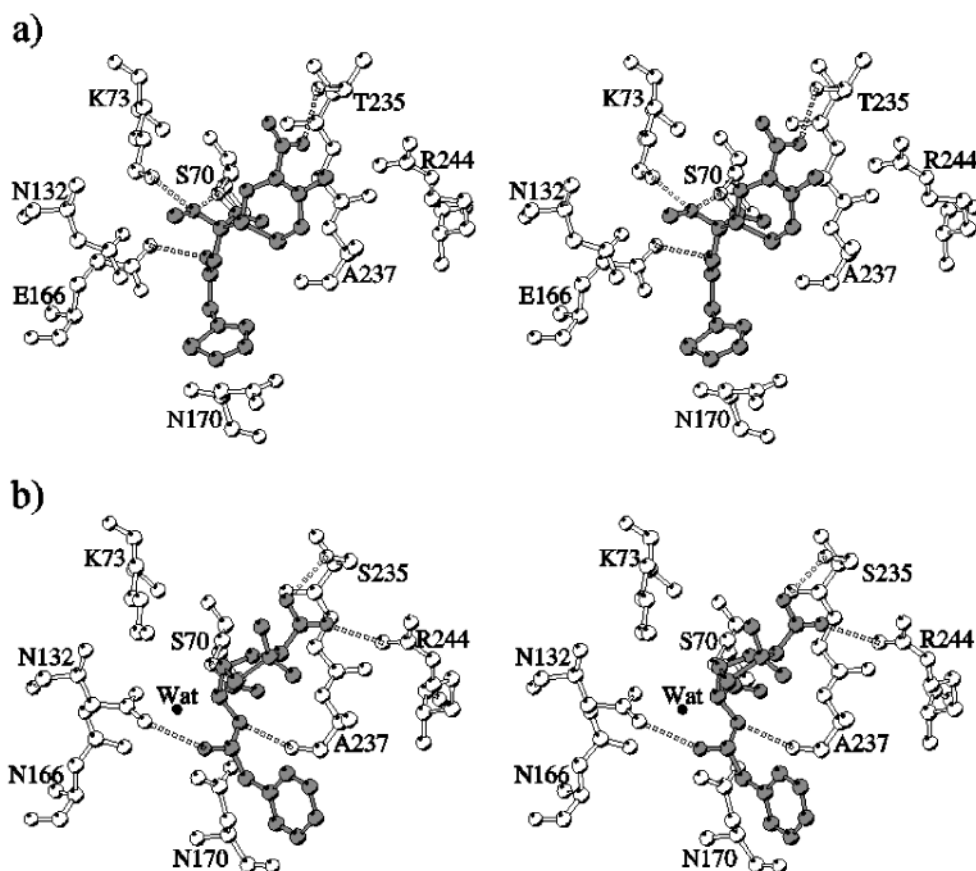

FIGURE 4: (a) Stereoview of the active site of the BS3−cefoxitin acyl−enzyme adduct. (b) Stereoview of the active site of the TEM-1−penicillin G acyl−enzyme adduct (24). Both stereoviews have the same orientation, and dashed lines represent hydrogen bonds.

is 2.6 Å from Glu166 OE1 and the hydrolytic Wat302 water molecule disappears. Accommodation of the 7β side chain of cefoxitin in the acyl−enzyme intermediate results in a modification of the Asn170 side chain conformation whose χ_1 and χ_2 torsional angles vary from −63.9° and −47.0° in the free enzyme to −170.1° and 34.2° in the cefoxitin adduct, respectively. This modification induces a slight motion of the Ω-loop (Pro167−Val172) (Figure 3).

At present, the only known acyl−enzyme adducts exhibiting a substrate-binding mode similar to that of the BS3−cefoxitin complex are the class C β-lactamase AmpC−moxalactam (31, 34) (PDB entry 1FCO for the wild-type

enzyme and PDB entry 1I5Q for the Asn152 → Ala mutant) and PBP2x−cefuroxime adducts (35) (PDB entry 1QMF). The wild-type AmpC−moxalactam crystal structure, with two molecules in the asymmetric unit, reveals two different positionings of moxalactam in the active site. In the first monomer, the substrate conformation is similar to that of cefoxitin in BS3, but in the second, the oxacephem ring has rotated by almost 180° around the C6−C7 bond, leading to van der Waals overlaps between Asn152 (equivalent to BS3 Asn132) and the α-methoxy group of moxalactam. This latter conformation would be impossible with a class A β-lactamase because of steric hindrance between the 7(α)(β) side

Table 4: Key Contacts in the BS3−Cefoxitin Adduct[a]

	protein/solvent atom	distance (Å)
cefoxitin atom		
C7	Ser70 OG	2.4
C8	Ser70 CB	2.4
O9	Ser70 N	2.9
O9	Ser70 OG	2.3
O9	Ala237 N	2.9
O9	Ala237 O	3.1
carboxylate		
O13	Ser130 OG	3.3
O13	Wat1344 O	2.8
O14	Thr235 OG1	2.6
O14	Gly236 N	3.4
O14	Arg244 NH1	3.5
7α side chain (R″)		
O16	Ser70 OG	2.3
O16	Lys73 NZ	2.6
O16	Ser130 OG	3.1
C17	Ser130 O	2.9
C17	Asn132 OD1	2.8
7β amido group		
O21	Ser70 OG	2.9
O21	Glu166 OE1	2.6

[a] The distances given are for the first monomer. The rms value for cefoxitin atoms in the two monomers when Cα atoms are superimposed is 0.14 Å.

chain and the Ω-loop. In the PBP2x−cefuroxime structure, the 7β-amido group of the inactivator adopts an orientation equivalent to that observed here for cefoxitin. However, in this case, the 7β-amido conformation is constrained rather by the steric hindrance of the 7β side chain than by the 7α substituent which is a mere hydrogen atom in cefuroxime. This acyl intermediate also induces movements of the active site bottom (Gln452) and of strand β3 (Thr550-Ala551-Gln552).

It is important to emphasize that in the BS3−cefoxitin structure, the α-methoxy group does not directly cause the conformational change but that it does so by influencing the 7β side chain orientation. In agreement with that, and as observed by NMR experiments, the 7β-formamidoyl-7α-methoxycephalosporanic acid does not induce structural modifications in the *B. licheniformis* 749/C β-lactamase.[2] Indeed, in this case, there is no steric incompatibility between the short 7β side chain and the Ω-loop. Nevertheless, for all compounds bearing a 7α-methoxy group, all steps of the hydrolysis pathway are severely impeded. To both accommodate the 7α and eventually the 7β side chains into the catalytic pocket and bring the substrate in a suitable position for the nucleophilic attack, the β-lactamase must necessarily undergo some conformational changes. The catalytic mechanism leading to formation of the acyl−enzyme complex is thus greatly impaired. Comparatively, the k_{cat}/K_m value determined for BS3 and cephalothin is more than 10^5-fold larger than with a similar substrate bearing a 7α-methoxy group (Table 1). Similarly, the deacylation process is also impaired by the introduction of a new hydrogen bonding scheme, which directly involves essential amino acid residues such as Ser70, Lys73, and Glu166, and by the disappearance of the hydrolytic water molecule.

The flexibility of class A β-lactamase active site has also been illustrated by the structure of the intermediate formed

Table 5: Kinetic Parameters

	k_{cat}/K_m (mM^{-1} s^{-1})			
enzyme[a]	penicillin G	cephalothin	cefoxitin	motif
BS3[b]	83000	14000	0.060	SDN132/KTGA237
TEM-1	84000	570	0.006	SDN132/KSGA237
MFO	1000	1900	0.016	SDN132/KTGS237
NMC-A	9300	15200	62.3	SDN132/KTGS237
SCLA	32	0.7	97	SDG132/KTGA237
P99	23000	20000	2500	YAN152/KTGS318

	k_2/K' (M^{-1} s^{-1})			
enzyme[a]	penicillin G	cephalothin	cefoxitin	motif
K15	150	2	860	SGC98/KTGS216
R61	13000	3000	1500	YSN161/HTGT301
PBP2x	58000	ND[c]	700	SSN397/KSGT550

[a] Second-order rate constants k_{cat}/K_m for the acylation of class A β-lactamases from *B. licheniformis* BS3, *E. coli* TEM-1 (*38*, *39*), *Mycobacterium fortuitum* (MFO) (*40*, *41*), *E. coli* NOR-1 (NMC-A) (*42*), and *S. clavuligerus* (SCLA) (*43*) and for the class C β-lactamase from *Enterobacter cloacae* P99 (*44*). For the DD-peptidases from *Streptomyces* K15 (*45*) and *Streptomyces* R61 (*46*) and for the PBP2x from *S. pneumoniae* (*47*), the second-order rate constants are described by the k_2/K' values. [b] Kinetic parameters were determined at 30 °C in 50 mM sodium phosphate at pH 7. [c] Not determined, but k_2/K' values for cephaloglycin, cephaloridine, and cefotaxime were determined to be 12 400, 93 000, and 162 000 M^{-1} s^{-1}, respectively (*47*).

after acylation of the TEM-1 β-lactamase by imipenem (*36*) (PDB entry 1BT5). This structure revealed a shift of the Met129−Asp131 loop accompanied by a conformational rearrangement of Ser130 forced by the 6α-1(*R*)-hydroxyethyl substituent. In that case, as in that of the TEM-1−6α-(hydroxymethyl)penicillanic acid adduct (*37*) (PDB entry 1TEM), it is essentially the deacylation step that is deficient because of the displacement of the hydrolytic water molecule by the substrate in the acyl−enzyme adduct.

DISCUSSION

To highlight the role suggested for the residue at position 132 (or the equivalent residue), kinetic parameters characterizing the interactions between β-lactams and some penicilloyl serine transferases are listed in Table 5. Only three representative β-lactams (penicillin G, cephalothin, and cefoxitin) are considered, and the structures of all the described enzymes are known, except for that of the class A β-lactamase from *Streptomyces clavuligerus*. As the kinetic data are compiled from independently published reports and were thus determined under different conditions, only a semi-quantitative analysis can be performed. Nevertheless, it clearly appears that the relative activities of all enzymes against penicillin G and cephalothin are much higher than against cefoxitin, except for that of the *S. clavuligerus* class A β-lactamase (*43*) and for the *Streptomyces* K15 DD-transpeptidase (*45*, *48*) (PDB entry 1SKF). For these two enzymes, where Asn132 is replaced with Gly and Cys, respectively, the steric constraints in the active site are significantly reduced and result in an easier accommodation of the α-methoxy group. On the other hand, without the stabilizing interactions between the 6β or 7β side chain of classical compounds such as penicillin G or cephalothin and Asn132, formation of the acyl−enzyme adduct is greatly impaired, as highlighted by the very poor acylation rates displayed by all substrates of the *S. clavuligerus* enzyme,

where the Gly132 residue is unable to form a hydrogen bond with the substrate side chain. For the class A NMC-A β-lactamase, the relative decrease of k_{cat}/K_m for cefoxitin compared to that of cephalothin is markedly less important than for the other class A enzymes characterized by a Ser130-Asp131-Asn132 motif (*42*). This difference in the substrate profile is due to an enlargement of the catalytic pocket, resulting of a shift of Asn132 of ~1 Å away from strand $\beta3$ (*49*) (PDB entry 1BUE). As shown in the acyl−enzyme structure of the NMC-A−imipenem adduct (*50*) (PDB entry 1BUL), the new position of Asn132 results not only in a more accessible active site for substrates with C6(C7)-α-substituents such as imipenem and cefoxitin but also in new possible hydrogen bonds between the residue 132 side chain and these substituents.

Some conclusions about the acylation pathway can be tentatively drawn on the basis of the structure of the BS3−cefoxitin adduct. If cephalothin is docked in the BS3 active site using the R61−cephalothin and/or the TEM-1−penicillin G adducts as templates, the absence of the C7 methoxy group allows a slight rotation around the antibiotic C7−C8 bond. It is possible to position the β-lactam carbonyl oxygen in the oxyanion hole and to simultaneously create interactions between the C4 carboxylate and Thr235, and between the antibiotic side chain CO and Asn132. The importance of this latter interaction is underlined by the observation that 7-aminocephalosporanic acid is a very poor substrate of the closely related 749/C enzyme (k_{cat}/K_m = 330 M^{-1} s^{-1}, i.e., 0.01% of that of cephalothin) and of all class A β-lactamases (*51*). It can thus be hypothesized that the interaction between the β-lactam side chain and Asn132 is crucial for a catalytically efficient positioning of the cephalosporin β-lactam ring. With cefoxitin, this favorable interaction is made impossible by the presence of the 7α-methoxy group, and in addition, the new interactions between this group and Ser70 and Lys73, with the disappearance of the catalytic water molecule, create important electronic perturbations in the active site, thus severely impairing both acylation and deacylation processes.

Conversely, the *Enterobacter cloacae* P99 class C β-lactamase (*52*) (PDB entry 2BLT), the *Streptomyces* R61 DD-carboxypeptidase (*53*) (PDB entry 3PTE), and the *Streptococcus pneumoniae* PBP2x (*35*) seem to be better adapted to the presence of an α-methoxy side chain than the class A β-lactamases (*44, 46, 47*). In all these structures, the conformation of the asparagine residue (Asn152, Asn161, and Asn397, respectively) is less restrained than the equivalent class A Asn132. The conformational freedom of the latter is strongly reduced by the class A Ω-loop (in particular by Glu166 as shown by the AmpC−moxalactam structure) and by the loop of residues 104 and 105 which covers the Ser130-Asp131-Asn132 motif at the entrance of the catalytic pocket.

It is also interesting to note that 6-aminopenicillanic acid is generally a much better substrate than 7-aminocephalosporanic acid for class A β-lactamases (*51*). This suggests that the interaction between the Asn132 NH$_2$ group and the antibiotic side chain CO is less important with the penam class of substrates, a conclusion which is reinforced by the fact that the cephalosporinase activity of the Asn132 → Ser mutant of the *S. albus* G β-lactamase is much more impaired than its penicillinase activity (*54*). However, the very poor

activity of both the Asn132 → Ala mutant of the same enzyme and of the *S. clavuligerus* β-lactamase toward all the substrates underlines the importance of the formation of a hydrogen bond with the residue in position 132. On the other hand, a better cephalosporinase activity can be related to the presence of an hydroxylated residue at position 237 (Table 5). A serine or threonine residue, just after the Lys-Thr(Ser)-Gly motif, would facilitate the binding of cephalosporins in the catalytic pocket by interacting with their carboxylate group. In the structures of the adducts formed by the *Streptomyces* R61 DD-carboxypeptidase and cephalothin or cephalosporin C, the carboxylate oxygen atoms are always hydrogen-bonded to the hydroxyl groups of the threonine residue of the His298-Thr299-Gly300 triad and Thr301. The same interactions occur in the PBP2x−cefuroxime acyl−enzyme adduct but with a serine residue instead of a threonine in the Lys547-Ser548-Gly549 motif.

In short, the previously discussed observations underline two major anchor sites of β-lactam substrates in the catalytic pocket of penicilloyl serine transferases. The first one implies the existence of the interaction between the Asn132 residue (or its equivalent) and the 7(6)β side chain and the second one the binding of the β-lactam carboxylate. The combination of these two interactions, which together contribute to an adequate substrate positioning, is probably one of the major factors that determine the catalytic efficiency of the enzyme toward its β-lactam substrates.

In light of all known three-dimensional structures, and especially of the structures of the adducts, a better understanding of kinetic results emerges which would lead to a more valuable estimation of the structure−activity relationship.

REFERENCES

1. Ghuysen, J.-M. (1994) *Trends Microbiol. 2*, 372−380.
2. Fisher, J., Belasco, J. G., Khosla, S., and Knowles, R. (1980) *Biochemistry 19*, 2895−2901.
3. Galleni, M., Amicosante, G., and Frère, J.-M. (1988) *Biochem. J. 255*, 123−129.
4. Jamin, M., Damblon, C., Bauduin-Misselyn, A.-M., Durant, F., Roberts, G. C. K., Charlier, P., Llabres, G., and Frère, J.-M. (1994) *Biochem. J. 301*, 199−203.
5. Citri, N., Kalkstein, A., Samuni, A., and Zyk, N. (1984) *Eur. J. Biochem. 144*, 333−338.
6. Faraci, S., and Pratt, R. (1986) *Biochemistry 25*, 2934−2941.
7. Matagne, A., Lamotte-Brasseur, J., Dive, G., Knox, J. R., and Frère, J.-M. (1993) *Biochem. J. 293*, 607−611.
8. Ledent, P., Duez, C., Vanhove, M., Lejeune, A., Fonzé, E., Charlier, P., Rhazi-Filali, F., Thamm, I., Guillaume, G., Samyn, B., Devreese, B., Van Beeumen, J., Lamotte-Brasseur, J., and Frère, J.-M. (1997) *FEBS Lett. 413*, 194−196.
9. Leslie, A. G. R. W. (1996) *MOSFLM Version 5.40 Mosflm Users Guide*.
10. Collaborative Computational Project No. 4 (1994) *Acta Crystallogr. D50*, 760−763.

11. Quillin, M. L., and Matthews, B. W. (2000) *Acta Crystallogr. D56*, 791−794.

12. Knox, J. R., and Moews, P. C. (1991) *J. Mol. Biol. 220*, 435−455.

13. Navaza, J. (1994) *Acta Crystallogr. A50*, 157−163.

14. Brünger, A. T. (1993) *X-PLOR Version 3.1: A System for X-ray Crystallography and NMR*, Yale University Press, New Haven, CT.

15. Roussel, A., and Cambillau, C. (1989) *Silicon Graphics Geometry Partner Directory*, pp 77−78, Silicon Graphics, Mountain View, CA.

16. Tatewaki, H., and Huzinaga, S. J. (1980) *Comput. Chem. 1*, 205−228.

17. Dive, G., Dehareng, D., and Ghuysen, J.-M. (1993) *Theor. Chim. Acta 85*, 409−421.

18. Frisch, M. J., et al. (1995) *Gaussian 94*, revision E.2, Gaussian, Inc., Pittsburgh, PA.

19. De Meester, F., Joris, B., Reckinger, G., Bellfroid-Bourguignon, C., Frère, J.-M., and Waley, S. G. (1987) *Biochem. Pharmacol. 36*, 2393−2403.

20. Kabsch, W., and Sander, C. (1983) *Biopolymers 22*, 2577−2637.

21. Kraulis, P. J. (1991) *J. Appl. Crystallogr. 24*, 946−950.

22. Ambler, R. P., Coulson, A. F., Frère, J.-M., Ghuysen, J.-M., Joris, B., Forsman, M., Levesque, R. C., Tiraby, G., and Waley, S. G. (1991) *Biochem. J. 276*, 269−270.

23. Rhazi-Filali, F., Zaid, A., Ledent, P., Vanhove, M., Van Beeumen, J., and Frère, J.-M. (1996) *FEMS Microbiol. Lett. 140*, 61−64.

24. Strynadka, N. C. J., Adachi, H., Jensen, S. E., Johns, K., Sielecki, A., Betzel, C., Sutoh, K., and James, M. N. G. (1992) *Nature 359*, 700−705.

25. Chen, C. C. H., Rahil, J., Pratt, R. F., and Herzberg, O. (1993) *J. Mol. Biol. 234*, 165−178.

26. Maveyraud, L., Pratt, R. F., and Samama, J.-P. (1998) *Biochemistry 37*, 2622−2628.

27. Ness, S., Martin, R., Kindler, A. M., Paetzel, M., Gold, M., Jensen, S. E., Jones, J. B., and Strynadka, N. C. J. (2000) *Biochemistry 39*, 5312−5321.

28. Lobkovsky, E., Billings, E. M., Moews, P. C., Rahil, J., Pratt, R. F., and Knox, J. R. (1994) *Biochem. J. 303*, 555−558.

29. Caselli, E., Powers, R. A., Blaszczak, L. C., Wu, C. Y., Prati, F., and Stoichet, B. K. (2001) *Chem. Biol. 8*, 17−31.

30. Powers, R. A., Caselli, E., Focia, P. J., Prati, F., and Stoichet, B. K. (2001) *Biochemistry 40*, 9207−9214.

31. Patera, A., Blaszczak, L. C., and Stoichet, B. K. (2000) *J. Am. Chem. Soc. 122*, 10504−10512.

32. Kelly, J. A., Knox, J. R., Moews, P. C., Hite, G. J., Bartolone, J. B., and Zhao, H. (1985) *J. Biol. Chem. 260*, 6449−6458.

33. Kuzin, A. P., Liu, H., Kelly, J. A., and Knox, J. R. (1995) *Biochemistry 34*, 9532−9540.

34. Trehan, I., Beadle, B. M., and Shoichet, B. K. (2001) *Biochemistry 40*, 7992−7999.

35. Gordon, E. J., Mouz, N., Duée, E., and Dideberg, O. (2000) *J. Mol. Biol. 299*, 477−485.

36. Maveyraud, L., Mourey, L., Kotra, L. P., Pedelacq, J.-D., Guillet, V., Mobashery, S., and Samama, J.-P. (1998) *J. Am. Chem. Soc. 120*, 9748−9752.

37. Maveyraud, L., Massova, I., Birck, C., Miyashita, K., Samama, J.-P., and Mobashery, S. (1996) *J. Am. Chem. Soc. 118*, 7435−7440.

38. Guillaume, G., Vanhove, M., Lamotte-Brasseur, J., Ledent, P., Jamin, M., Joris, B., and Frère, J.-M. (1997) *J. Biol. Chem. 272*, 5438−5444.

39. Dubus, A., Wilkin, J. M., Raquet, X., Normark, S., and Frère, J.-M. (1994) *Biochem. J. 301*, 485−494.

40. Quinting, B., Reyrat, J.-M., Monnaie, D., Amicosante, G., Pelicic, V., Gicquel, B., Frère, J.-M., and Galleni, M. (1997) *FEBS Lett. 406*, 275−278.

41. Amicosante, G., Franceschini, N., Segatore, B., Oratore, A., Fattorini, L., Orefici, G., Van Beeumen, J., and Frère, J.-M. (1990) *Biochem. J. 271*, 729−734.

42. Mariotte-Boyer, S., Nicolas-Chanoine, M. H., and Labia, R. (1996) *FEMS Microbiol. Lett. 143*, 29−33.

43. Perez-llarena, F., Martin, J. F., Galleni, M., Coque, J. J., Fuente, J. L., Frère, J.-M., and Liras, P. (1997) *J. Bacteriol. 179*, 6035−6040.

44. Matagne, A., Dubus, A., Galleni, M., and Frère, J.-M. (1999) *Nat. Prod. Rep. 16*, 1−19.

45. Leyh-Bouille, M., Nguyen-Distèche, M., Pirlot, S., Veithen, A., Bourguignon, C., and Ghuysen, J.-M. (1986) *Biochem. J. 235*, 177−182.

46. Frère, J.-M., and Joris, B. (1985) *CRC Crit. Rev. Microbiol. 11*, 299−396.

47. Jamin, M., Hakenbeck, R., and Frère, J.-M. (1993) *FEBS Lett. 331*, 101−104.

48. Fonzé, E., Vermeire, M., Nguyen-Distèche, M., Brasseur, R., and Charlier, P. (1999) *J. Biol. Chem. 31*, 21853−21860.

49. Swarén, P., Maveyraud, L., Raquet, X., Cabantous, S., Duez, C., Pédelacq, J.-D., Mariotte-Boyer, S., Mourey, L., Labia, R., Nicolas-Chanoine, M.-M., Nordmann, P., Frère, J.-M., and Samama, J.-M. (1998) *J. Biol. Chem. 41*, 26714−26721.

50. Mourey, L., Miyashita, K., Swarén, P., Bulychev, A., Samama, J. P., and Mobashery, S. (1998) *J. Am. Chem. Soc. 120*, 9382−9383.

51. Matagne, A., Misselyn-Bauduin, A.-M., Joris, B., Erpicum, T., Granier, B., and Frère, J.-M. (1990) *Biochem. J. 265*, 131−146.

52. Lobkovsky, E., Moews, P. C., Liu, H., Zhao, H., Frère, J.-M., and Knox, J. R. (1993) *Proc. Natl. Acad. Sci. U.S.A. 90*, 11257−11261.

53. Kelly, J. A., Knox, J. R., Zhao, H., Frère, J.-M., and Ghuysen, J.-M. (1989) *J. Mol. Biol. 209*, 281−295.

54. Jacob, F., Joris, B., Lepage, S., Dusart, J., and Frère, J.-M. (1990) *Biochem. J. 271*, 399−406.